JOURNAL OF GEOPHYSICAL RESEARCH, VOL. 104, NO. C7, PAGES 15,843–15,857, JULY 15, 1999

Barents Sea seasonal ice zone features and processes from ERS 1 synthetic aperture radar: Seasonal Ice Zone Experiment 1992

Stein Sandven, Ola M. Johannessen,[1] Martin W. Miles,[1] Lasse H. Pettersson, and Kjell Kloster

Nansen Environmental and Remote Sensing Center, Bergen, Norway

Abstract. Sea ice features and processes in the Barents Sea were studied during the Seasonal Ice Zone Experiment 1992 (SIZEX92), a dedicated ERS 1 satellite synthetic aperture radar (SAR) field campaign carried out in March 1992. SIZEX92 was based around the research vessels *Polarsyssel* and *Håkon Mosby*. In situ oceanographic, meteorological, and ice measurements were made, coordinated with low-altitude aerial observations and ERS 1 SAR data acquired in near real time. Fifty-eight low- and full-resolution SAR scenes were obtained during SIZEX92, which provided a validation data set for ERS 1 SAR backscatter under winter conditions in the Barents Sea. Analysis of SIZEX92 data has provided geophysical insights, including a better understanding of Barents Sea ice edge freezing processes and ice edge development in response to atmospheric forcings. In particular, areas of new ice formation were found to be related to bathymetric features through their influence on the circulation of Arctic and Atlantic water masses. ERS 1 SAR image sequences revealed rapid, mesoscale variations in new ice areas and the ice edge in response to wind conditions. In addition to geophysical insight, SIZEX92 demonstrated some of the technical capabilities and limitations of ERS 1 SAR to identify new ice areas, the ice edge, ice floes, and ice types. Mapping new ice areas using satellite SAR data may be considered the most promising new application. The limitations of ERS-1 SAR-derived ice classification and ice motion estimates in the marginal ice zone are identified.

1. Introduction

The Barents Sea is the world's most northerly sea that is not covered with perennial ice, though its seasonal ice cover can be extensive in winter. The spatial and temporal variability of seasonal ice zone features and processes in the Barents Sea has been studied during oceanographic fieldwork [e.g., *Midttun*, 1985], by remote-sensing observations [e.g., *Vinje*, 1985], and with a combination of field and remote-sensing observations [e.g., *Sandven and Johannessen*, 1993].

The last mentioned is occasionally done via dedicated experiments, such as the second Marginal Ice Zone Experiment (MIZEX87) in winter 1987 and the first Seasonal Ice Zone Experiment (SIZEX89) in winter 1989. Those experiments combined in situ observations and coincident satellite images and airborne synthetic aperture radar (SAR) data. The latter are obtained essentially independent of weather and illumination. MIZEX87 and SIZEX89 demonstrated the usefulness of SAR for studying the sea ice cover in the Barents Sea [*Johannessen et al.*, 1992; *Sandven and Johannessen*, 1993]. During MIZEX87, the western Barents Sea was mapped for the first time using X band airborne SAR on 3 consecutive days. The high-resolution (15 m) SAR system provided detailed information on mesoscale ice edge circulation, including ice tongues and vortex pairs [*Johannessen et al.*, 1992]. It was also evident that SAR could provide at least qualitative information on features and processes related to convergence and divergence, as well as ice compactness and ice floe characteristics [*Sandven and Johannessen*, 1993]. Studies such as these indicated the great potential for satellite-based SAR to provide detailed, repetitive regional data on sea ice characteristics and their spatial and temporal variability.

The first European Remote Sensing Satellite (ERS 1) and its successor, ERS 2, have provided SAR data since 1991. The ERS 1 SAR operated from July 1991 to July 1996, providing regularly repetitive, high-resolution, C band (5.3 cm) images and backscatter data. The need for investigations dedicated to the validation of sea ice parameters derived from ERS 1 SAR was clearly indicated. Since its launch, such investigations have been made in regions such as the Baltic [*Carlström and Ulander*, 1995] and Greenland Seas [*Gudmandsen et al.*, 1995]. The purpose of this paper is to report the geophysical and technical results of SIZEX92, a major field and remote sensing investigation carried out using ERS-1 SAR data in the Barents Sea seasonal ice zone, with primary emphasis on ice edge features and processes and secondary emphasis on ice classification and ice motion in the marginal ice zone.

2. Barents Sea Physical Environment

2.1. Barents Sea Oceanography

The Barents Sea is a shallow marginal Arctic sea, with an area of about 1.4 x 10^6 km^2, situated between northwestern Europe, Svalbard, Franz Josef Land, and Novaya Zemlya

[1]Also at Geophysical Institute, University of Bergen, Norway

Paper number 1998JC900050.
0148-0227/99/1998JC900050$09.00

(Figure 1). Here only a brief overview of the Barents Sea is provided; more comprehensive discussions are given by *Midttun* [1989] and *Loeng* [1991]. The bathymetry is characteristic of the other shelf seas of the Arctic, with a mean depth of only 250 m and a maximum depth of only 500 m in the Bear Island trough near its western edge. The shelf breaks are more defined in the western Barents Sea than in the eastern part.

The major currents and water masses are reviewed by *Loeng* [1991] and *Pfirman et al.* [1994]. Figure 1 indicates the generalized surface currents. Alongside the Norwegian Coastal Current, the Norwegian Atlantic Current is a continuation of part of the North Atlantic Current. Off the northern coast of the Norway, the current branches northward and eastward. These currents bring relatively warm coastal and Atlantic Water into the Barents Sea.

The inflow of Arctic Water to the Barents Sea occurs mainly along two routes, between Svalbard and Franz Josef Land and between Franz Josef Land and Novaya Zemlya. The first mentioned flows mainly as the East Spitsbergen Current, and the latter flows as the Persey Current. The boundary zone between the Atlantic and Arctic water masses is the oceanic polar or Arctic front. In the western Barents Sea, the front is relatively well defined, and its location is related to bottom topography [*Johannessen and Foster*, 1978; *Harris et al.*, 1998]. In the eastern part, the front is less distinct, with large areas of mixed Atlantic and Arctic water.

2.2. Barents Sea Ice Regime

An overview of the Barents Sea ice cover is given by *Vinje and Kvambekk* [1990]. In summer, the Barents Sea is usually ice free to between 77° and 82°N in August, at its minimum extent. In winter, the sea ice cover is never total, but it can be extensive. The winter maximum ice extent varies much more than the summer minimum, both in magnitude and timing [*Gloersen et al.*, 1992]; the interannual variability of the late winter ice cover is indicated in Figure 1.

Analysis of digitized ice charts identified a decreasing trend in the Barents Sea ice extent during the period 1966-1988 [*Vinje and Kvambekk*, 1990], and its spatial variability during the period 1979-1987 was revealed by *Parkinson* [1991] and *Gloersen et al.* [1996] using satellite passive microwave data. *Gloersen et al.* [1996] found the largest reductions, greater than 40% locally, in ice concentration in the entire Arctic to be in the eastern Barents Sea and north of Svalbard, though the trends since 1987 have not been determined.

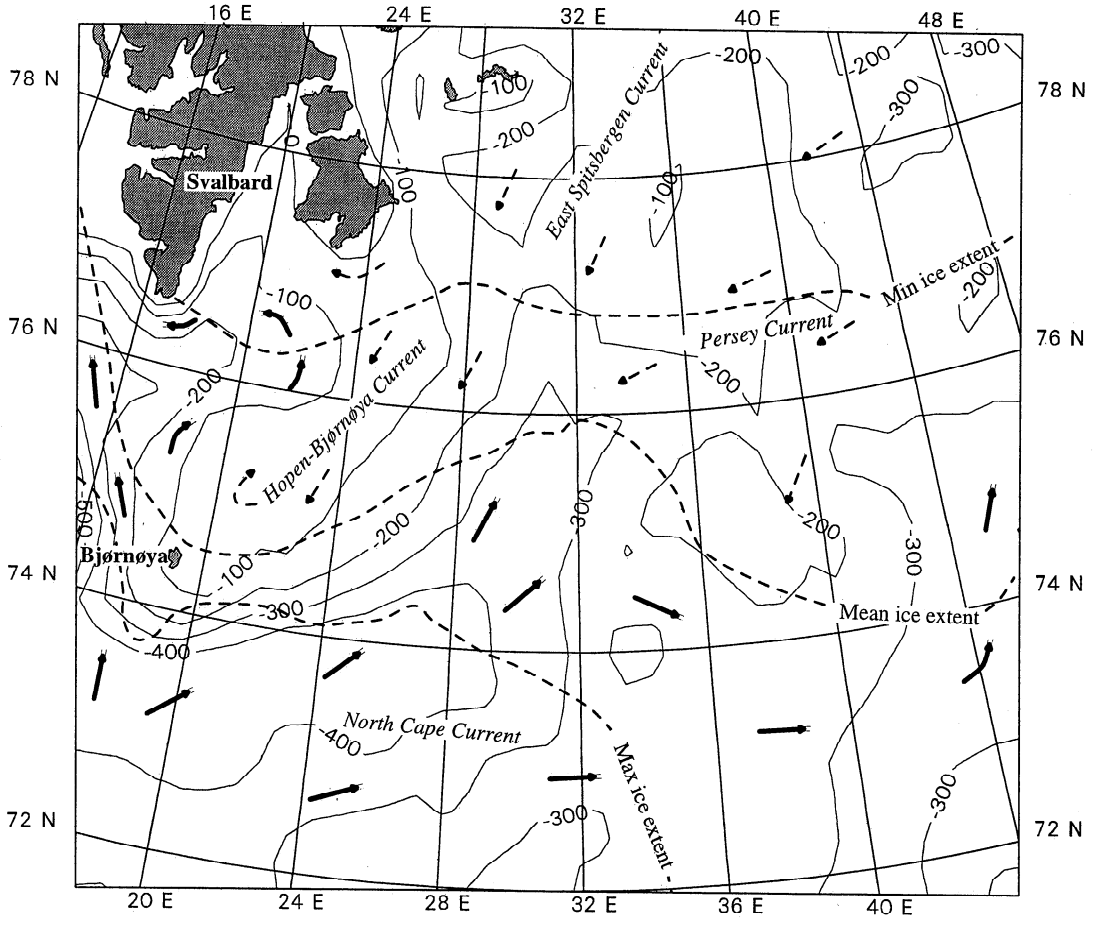

Figure 1. Map of the Barents Sea indicating bathymetry, surface currents, water masses, and winter sea ice cover. The isobaths (solid lines) are at 100-m intervals. The major surface currents are labeled and indicated by arrows (not proportional to current speed); solid arrows are warm currents (Atlantic Water), and dashed arrows are cold currents (Arctic Water). The three dashed lines indicate, from north to south, the minimum, mean, and maximum winter sea ice extent, based on a climatology from *Vinje and Kvambekk* [1990]. The shaded area at top left is Svalbard.

The formation of sea ice during the cold season is determined by the atmospheric and oceanic circulation features that result in the cooling of surface water masses. The Barents Sea Low appears to be particularly important, with its effect on the prevailing wind directions more or less determining the ice edge position [*Vinje and Kvambekk*, 1990]. In addition to sea ice, the Barents Sea contains icebergs originating from glaciers on Franz Josef Land.

Ice drift in the Barents Sea has been studied using drifting buoys and satellite observations in conjunction with meteorological data [e.g., *Vinje*, 1985]. In contrast to the Greenland Sea, ice drift in the Barents Sea is predominantly wind driven [*Vinje and Kvambekk*, 1990]. Accordingly, interannual variations in synoptic-scale atmospheric circulation affect the exchange of ice between the Barents and Kara Seas and the Arctic Ocean proper.

3. SIZEX92: Seasonal Ice Zone Experiment 1992

3.1. SIZEX92 Strategy

The usefulness of airborne SAR demonstrated in the prelaunch experiments MIZEX87 and SIZEX89 heightened expectations for the advent of ERS 1 SAR in July 1991. The need for investigations dedicated to the validation of ERS 1 SAR-derived sea ice parameters in the Barents region was indicated. Toward this end, two validation experiments were made in the Barents Sea near Svalbard, in summer and winter conditions.

SIZEX91 was a small pilot investigation made north of Svalbard in August 1991, shortly after the launch of ERS-1 [*Frette et al.*, 1992]. The SIZEX91 observations made from the research vessel *Lance* provided an in situ data set for preliminary validation of ERS 1 SAR data obtained under summer conditions.

SIZEX92 was a more intensive investigation dedicated to (1) the validation of ERS 1 SAR-derived sea ice parameters in winter conditions and (2) studying the variability of various oceanographic and sea ice features and processes in the region. The experiment was carried out in the western Barents Sea between 75° and 79°N (Figure 2), both outside and inside the winter ice edge. It was a coordinated investigation involving two research vessels (the R/V *Håkon Mosby* and the ice-strengthened R/V *Polarsyssel*), low-altitude helicopter and airplane observations, and satellite data from ERS 1 SAR. SIZEX92 also served to demonstrate the usefulness of near-real-time ERS 1 SAR data to help direct the field investigation in progress. This was the first time that such a system was used in a sea ice field investigation.

3.2. Field Data

The *Håkon Mosby* operated outside the main ice edge during the experiment (Figure 2). The vessel conducted a detailed hydrographic survey by conventional conductivity-temperature-depth (CTD) measurements as well as by CTD aboard a Seasor, a towed CTD that undulates between the surface and about 200 m depth. Data from a total of 152 CTD stations were obtained from March 1-5, 1992. Water current velocity sections were made using an acoustic Doppler current profiler (ADCP). Two bottom-moored current meter rigs were also deployed. Shipboard observations and photographs of newly formed ice were taken. Meteorological measurements were made every 3 hours using a coastal climate weather station and other instruments for a detailed survey of the planetary boundary layer.

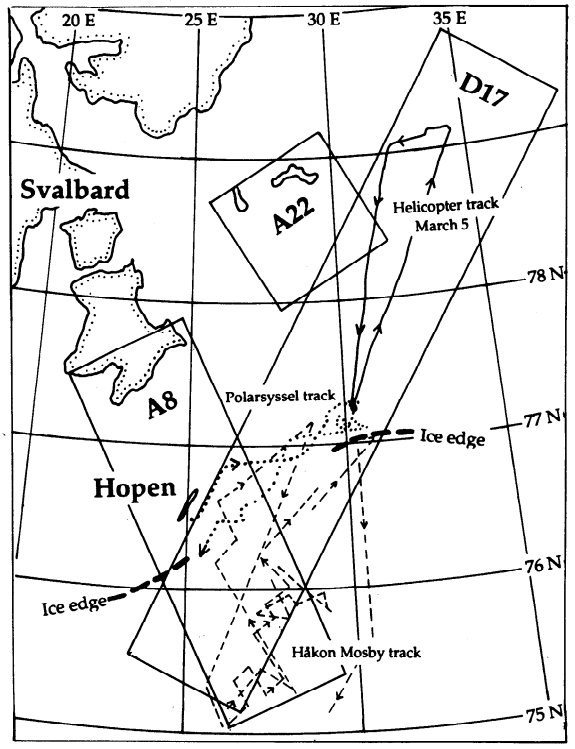

Figure 2. Map of the Seasonal Ice Zone Experiment (SIZEX92) study area in the western Barents Sea, March 1992. Indicated are the tracks of the R/Vs *Polarsyssel* and *Håkon Mosby*, as well as a helicopter flight. The coverage of the ERS 1 synthetic aperture radar (SAR) swaths used during the experiment is indicated by the boxes; the numbers refer to the particular ascending (A) and descending (D) ERS 1 paths.

The *Polarsyssel* operated 15-30 km into the ice pack east of Hopen (Figure 2). From there, a helicopter flew along an ERS 1 SAR swath to obtain observations of the ice conditions and to provide access to large ice floes and icebergs farther into the ice pack. In situ samples and measurements were taken at various first-year and multiyear floes and from a large tabular iceberg, presumed to be from Franz Josef Land. The ship-based helicopter made observations nearly every day, providing a global positioning system (GPS) registered, downward looking video record of ice below, complemented by a sequence of aerial photographs taken on March 8, 1992, from an altitude of 6300 m.

3.3. ERS 1 SAR Data

The SIZEX92 field observations were complemented by near-coincident high- (16 x 20 m pixels) and low-resolution (100 m pixel) ERS 1 SAR data, ordered prior to the experiment. The temporal differences between the SAR and in situ data varied from simultaneous to up to about 24 hours, depending on the particular in situ observations. The SAR scenes were acquired along one descending and two ascending swaths (Figure 2). Forty-eight low-resolution and 10 full-resolution scenes were obtained. As part of the experiment, the data were received aboard the research vessels in near real time via the Tromsø Satellite Station (TSS), then transferred to the Nansen Environmental and

Remote Sensing Center (NERSC). There the images were manually interpreted and sent to the research vessels in the experiment area less than 3 hours after the satellite overpass. The images were used to identify the ice edge and potential multiyear ice floes for *in situ* investigation.

After the field experiment, backscatter data were normalized in range to an incidence angle of 23° (in the center of the swath) by applying corrections for antenna pattern, slant-to-ground effect and slant range, as described by the European Space Agency (ESA) [*Laur et al.*, 1997]. Then the digital values V in the images were converted to σ_0 values by the relation $\sigma_0 = 20 \log V - 46.9$. The lowest backscatter (grease ice) observed in the image data had values of $V = 14$, and this was assumed to represent the noise floor given by ESA to be -24 dB. The accuracy of this calibration is estimated to be 1-2 dB, which is lower than the 1 dB or better accuracy estimates more recently given by ESA, because no corner reflectors or transponders were available at that time.

3.4. Meteorological Conditions and Ice Edge Position

The Barents Sea is often exposed to low-pressure systems, especially in winter, when cyclones are frequently advected from the North Atlantic along predominantly northeasterly tracks [*Rogers and Moseley-Thompson*, 1995]. The variable wind conditions and associated ocean wave fields are important forcing mechanisms on the sea ice cover, affecting the position and configuration of the ice edge and the formation and development of new ice.

In the week before the start of SIZEX92, easterly winds up to 10 m s^{-1} prevailed in the Hopen area (Figure 2), and the ice edge was situated parallel to the Bjørnøya (Bear Island) channel, as is typical in winter. From February 22 to March 2, 1992, the ice edge east of Hopen was displaced about 100 km northward. Consequently, the ice edge region was very compact at the start of the experiment. After March 2, 1992, the ice edge relaxed somewhat and moved 20-50 km southward (see section 5). During the experiment, the air temperature varied between -2° and -25°C, and only short periods of low visibility prevented helicopter operations.

3.5. Characterization of Ice Conditions from SAR Images

Previous field and remote sensing investigations have indicated that the Barents Sea seasonal ice zone sometimes contains all the major ice types (multiyear, first-year, young, and new ice) as well as icebergs [*Vinje and Kvambekk*, 1990]. However, the detailed distribution and spatial and temporal variability of the ice types are not well known owing to a lack of requisite observations. With frequently obtained SAR images of the area, it will be possible to investigate the ice type distribution in much more detail, as illustrated in the sequence of four ERS 1 SAR images (Figure 3). These images were obtained in the SIZEX92 experiment period, from March 2 to 11, covering the area where all the field observations were made.

A characteristic common to all of the images is that the main ice pack (top left), consisting of mostly first-year and some multiyear ice, is readily distinguished from areas of newly formed ice and open water. The boundary zone separating the ice pack from the newer ice can be identified by the former's more homogenous gray tones; this zone varies considerably in both position and configuration during the period. Within the ice pack, two different ice regimes become apparent in the SAR images. The first is an intermediate ice edge zone about 20-30 km wide characterized by many small floes, broken up by the incoming wave field in the previous days and weeks. This zone appears as a relatively uniform gray area in the SAR images without any identification of individual floes or other ice features. North of this zone is the interior of the ice pack, which has not been affected by surface waves. This area consists mostly of consolidated first-year ice with clusters of large multiyear floes (light gray image features) drifting southward from the Arctic Ocean proper. Some leads with new ice can also be found in this area because of their very dark appearance indicating low backscatter. On the basis of these observations, we have defined three different ice regimes or zones shown in Figure 4: (1) zone A, the interior of the ice pack, (2) zone B, the intermediate zone and (3) zone C, the ice edge zone. This division is useful in the further analysis of the SAR images, including ice classification (see section 6.1).

Another image characteristic is that the ice edge separating open water (homogenous light tones) from ice is evident is all of the images. The ice edge expands very rapidly during freezing, as seen in the images of March 2 and 5 (Figures 3a and 3b) when the edge moves up to 50 km to the southeast in only 3 days. The ice edge can also be compacted rapidly as the wind blows toward the edge, which is demonstrated in the March 8 and 11 images (Figures 3c and 3d). This new ice formation and ice edge development is investigated further in sections 4 and 5, respectively.

4. Ice Edge Freezing Processes

4.1. Freezing Processes: Background

Sea ice freezing processes have a key role in global thermohaline circulation, as ice formation and the associated brine rejection result in formation of deep water. The importance of freezing processes and deep water formation in the Greenland Sea is generally acknowledged [*Aagaard and Carmack*, 1989], although analysis of their interannual variability reveals remarkable irregularities in deep convection [*Alekseev et al.*, 1994]. In the Barents Sea, these processes have been much less studied, though it is known that sea ice formation in the fall and winter results in the in situ development of Arctic Water (as opposed to advection from the Arctic proper) as well as cold, saline, dense (> 28.3 σ_0) bottom water [*Midttun*, 1985; *Pfirman et al.*, 1994].

The main objective of the SIZEX92 *Håkon Mosby* cruise was to survey the oceanographic variability in the oceanic polar front area outside the Barents Sea ice edge, where coincident ERS 1 SAR data were obtained. Of particular importance were the acquisition and validation of data where cold Arctic Water encounters the warmer water southeast of Hopen and where freezing occurs near the ice edge.

4.2. Freezing Processes: Observations

In the first stage of new ice formation, the ocean surface is covered by frazil ice or grease ice which dampens the short surface waves (Figure 5), such that C band SAR imagery with radar wavelength of about 5 cm may have a unique capability to map areas of new ice. In areas where the short waves are dampened by new ice, the SAR backscatter is low. In ice-free

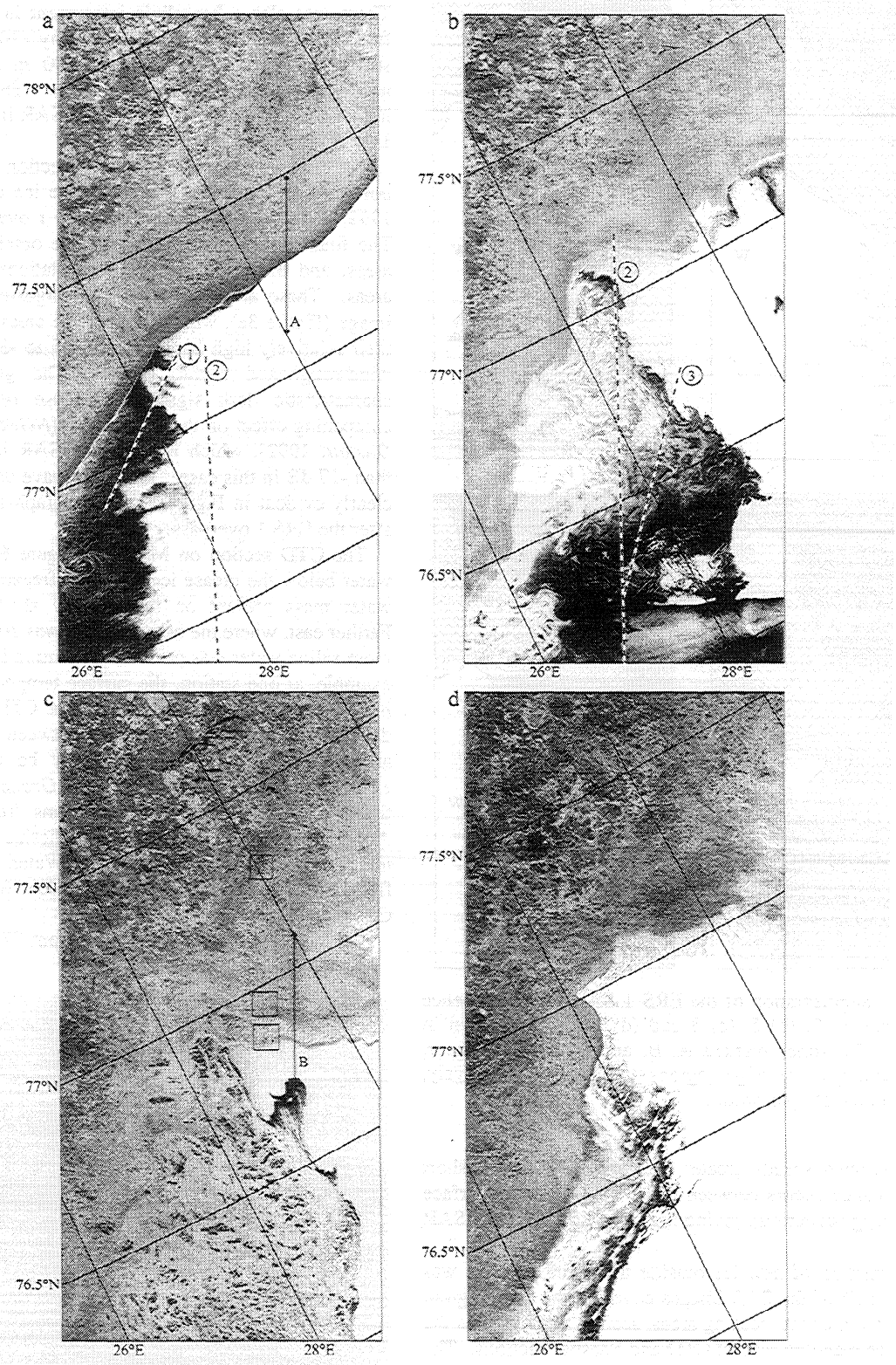

Figure 3. ERS 1 SAR images acquired on March (a) 2, (b) 5, (c) 8 and (d) 11, 1992, from the same descending path (D17 in Figure 2) in the western Barents Sea. Each image is made up of two 100- x 100-km ERS 1 SAR scenes. The sequence shows the movement, development, and reconfiguration of the ice edge. The locations of the backscatter profiles shown in Figure 9 are marked with arrows in Figures 3a and 3c. The locations of the conductivity-temperature-depth (CTD) sections shown in Figures 6-8 are marked with dashed lines in Figures 3a and 3b. The locations of the low-altitude aerial photographs shown in Figures 10, 12 and 13 are marked with squares in Figure 3c. ERS 1 SAR data are © ESA 1992.

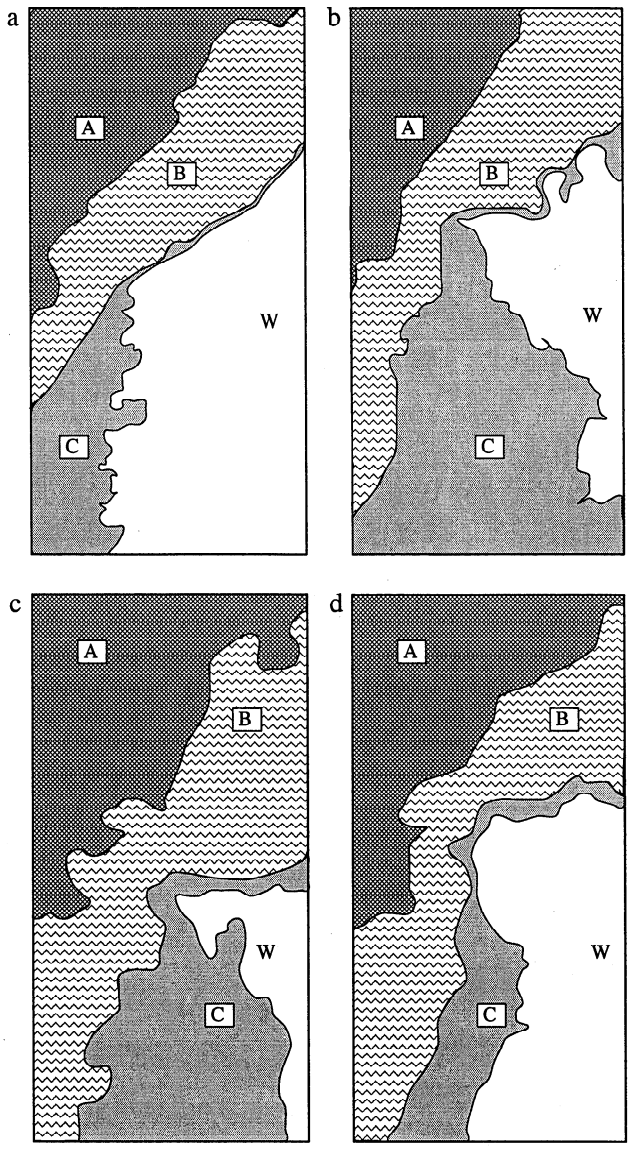

Figure 4. Segmentation of the ERS 1 SAR image sequence from March (a) 2, (b) 5, (c) 8 and (d) 11, 1992, shown in Figure 3. The zones marked A, B, and C are the interior, intermediate, and ice edge regions (see text), respectively, while W indicates open water.

waters and wind speeds greater than about 2-3 m s^{-1}, short wave resonance occurs between radar waves and the surface waves (Bragg scattering), giving high backscatter in the SAR images.

The formation of new ice outside the main ice edge was observed in all of the SAR images covering the edge region. Documentation of the freezing areas, seen as dark areas in the images, was made by several CTD and Seasoar sections. The initial crossing of the polar front was made on March 1-2, 1992. The front was clearly evident from the ADCP and Seasoar sections, which revealed a sharp transition from Atlantic Water (temperature $T \approx 0.75$°C and salinity $S \approx 34.55$‰) to Arctic Water ($T < -1.75$°C and $S < 34.55$‰). The front was located about the 200-m isobath, and was wedge shaped, with a near-surface frontal zone of about 40 km, decreasing to about 15 km at 100 m depth. The ADCP-measured current velocities near the surface were < 10 cm s^{-1} in the Arctic Water and > 10 cm s^{-1} in the Atlantic Water. There was also a baroclinic jet current in the center of the front zone, with a maximum velocity (30 cm s^{-1}) near the surface; the jet extended below 100 m and was directed northward along the 200-m isobath. There was no clear indication of the front on the ERS 1 SAR images from March 1-2, 1992.

North of the polar front, a CTD section was obtained in a northeasterly direction parallel to the ice edge on March 2, 1992, just 2 to 6 hours after an ERS 1 overpass (Figure 3a). The four southernmost stations were obtained in grease ice areas, and the three northernmost stations were in ice-free areas. These areas are readily distinguishable on the SAR image (Figure 3a), where the ice-free areas are evidenced by their relatively high backscatter (-4.5 to -3.0 dB) caused by wind-roughened surface waves. The grease ice has a characteristic dark signature because of its short wave dampening effect on the sea surface [*NORSEX Group*, 1983; *Onstott*, 1992], which reduced the SAR backscatter to less than -17 dB in this case. The short wave dampening effect is clearly evident in Figure 5, a photograph taken just 3 hours after the ERS 1 overpass.

The CTD section on March 2 (Figure 6) showed that the water below the grease ice was near-freezing Arctic Water, a water mass present on the shallow shelf east of Hopen. Farther east, where the bottom depth was 200-300 m, warmer, more saline water was present, preventing ice formation. For example, at one station, the surface temperature was -1.4°C, increasing to 1.3°C below 150 m. The CTD and ERS 1 SAR data show a high correspondence between water masses and areas of freezing, which then may be used to map the extension of Arctic Water [*NORSEX Group*, 1983], assuming that most of the local sea ice forms from Arctic Water. Although *Harris et al.* [1998] hypothesize that fresh surface meltwater, i.e., modified Atlantic Water, is the source of freezing in this area, this is not evident from the SIZEX92 CTD data.

A long CTD section (Figure 7), from 77°10′N to 75°20′N

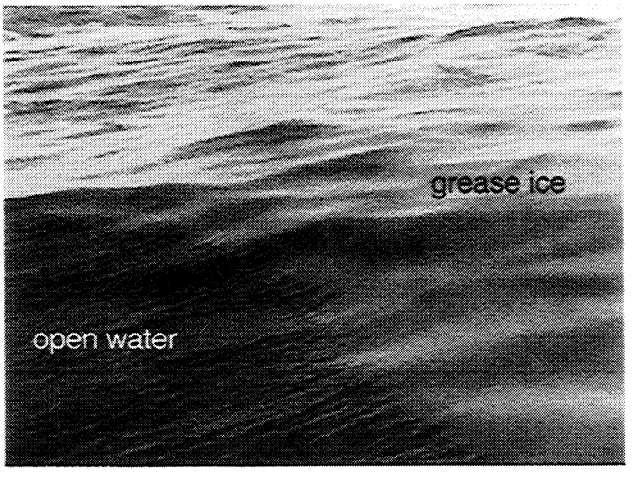

Figure 5. Oblique photograph of newly formed grease ice taken from the *Håkon Mosby* on March 2, 1992. The wave-dampening effect of grease ice is clearly evident by comparing the surface roughness on either side of the boundary between open water (bottom left) and grease ice (right). The wavelength of the short waves at bottom left is 10-20 cm.

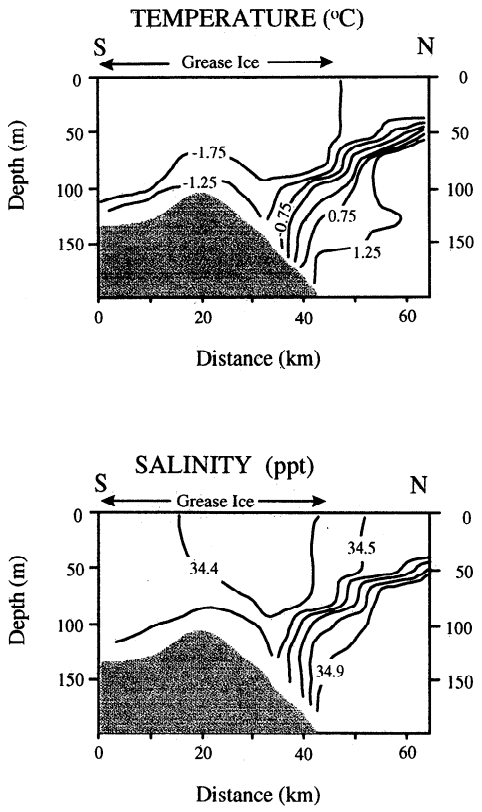

Figure 6. CTD section taken by the R/V *Håkon Mosby* on March 2, 1992, between 2 and 6 hours after an ERS 1 overpass (see Figure 3a). Indicated are (top) temperature and (bottom) salinity. The shaded areas are the seafloor.

was obtained by the *Håkon Mosby* during the night of March 3, 1992. An ERS 1 SAR image from the previous day showed no grease ice in this particular area. However, during the night, grease ice was observed (from the ship) to form in part of the section, north of 76°20'N. An ERS 1 SAR image (Figure 3b) obtained 2 days later (March 5, 1992) indicated that this area was by then completely covered with newly formed ice. The section (Figure 7) revealed a 60- to 80-m deep surface layer of near-freezing water ($T \approx -1.75$°C, $S < 34.5$‰), upon which grease ice was observed to form. This cold water was located over a shallow (approximately 150 m) ridge. Further south was a trench (> 200 m), where warmer Atlantic Water ($T > 1.0$°C, $S > 34.90$‰) was found at depths below 50 m; the Atlantic Water appeared to be steered by the bottom topography.

Another CTD section (Figure 8) across the tongue of grease ice was made on March 5, 1992, coincident with a SAR image (Figure 3b). The section crossed a tongue of new ice (grease ice and pancake ice) readily seen in the SAR image. The *Håkon Mosby* started inside the ice tongue and moved out to open water, then turned back into the ice and took several stations in the ice edge region. The water mass below the ice tongue was Arctic Water near its freezing point and salinity less than 34.50‰. It occupied most of the water column in the shallow area 100-150 m deep. Northeast of the ice tongue, the surface water was warmer (> -1.5°C) and more saline (> 34.50‰), such that freezing occurred just when the surface temperature was near -1.8°C and not higher. North of the ice tongue, warmer Atlantic Water (> 1.25°C) penetrated northward below the surface layer.

The sequence of CTD sections provided documentation of the areas of freezing near the western Barents ice edge, by

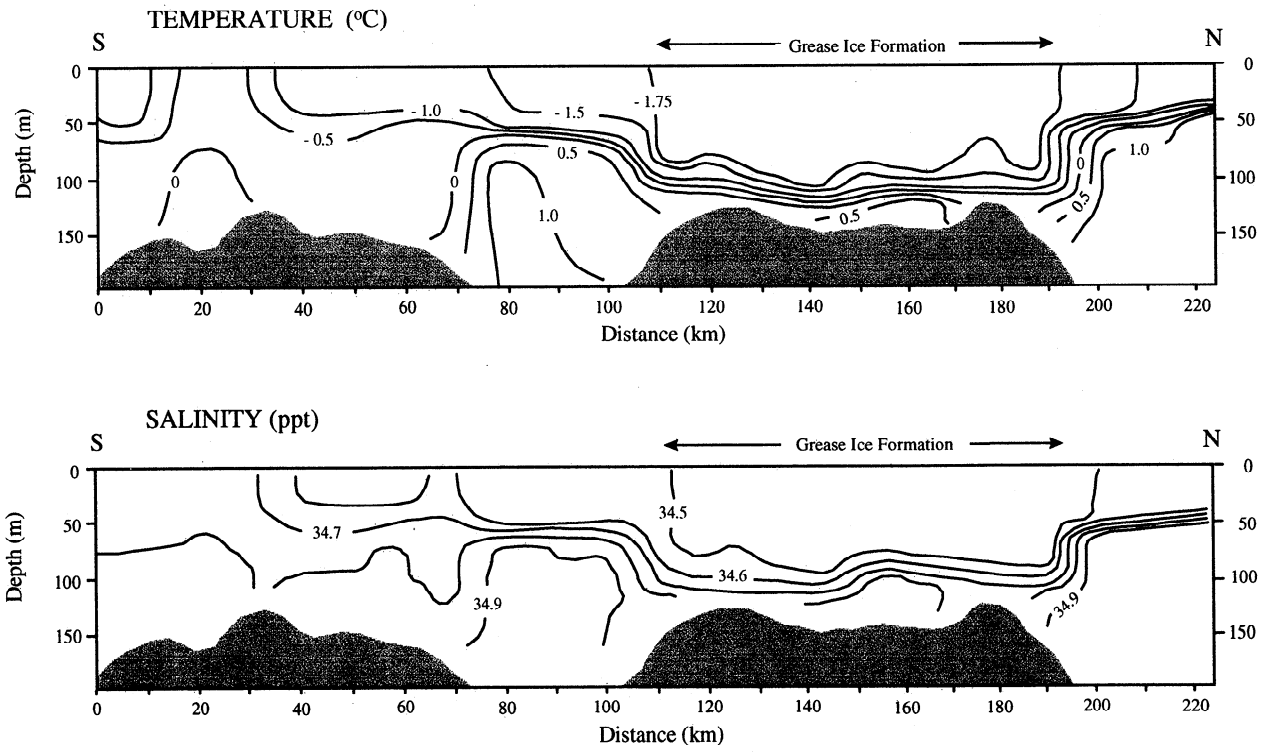

Figure 7. CTD section taken by the R/V *Håkon Mosby* on March 3, 1992. Indicated are (top) temperature and (bottom) salinity. The shaded areas are the seafloor.

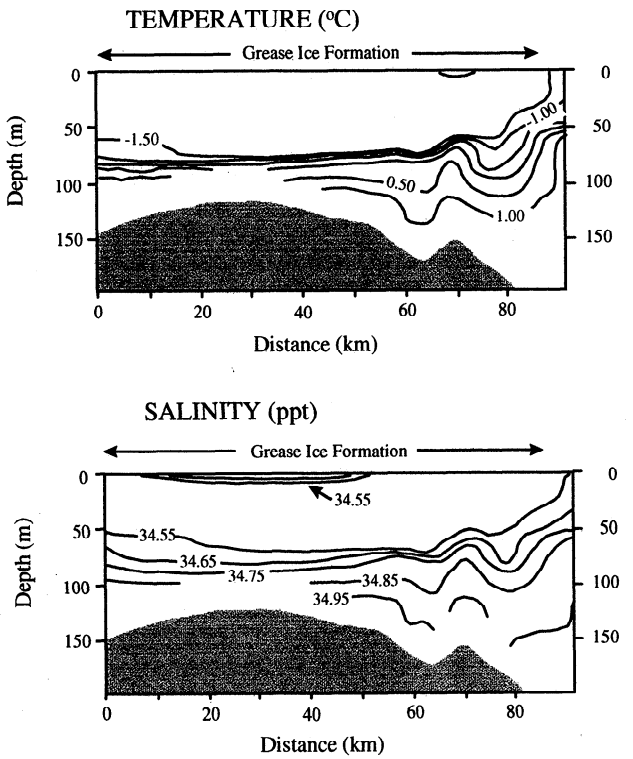

Figure 8. CTD section taken by the R/V *Håkon Mosby* on March 5, 1992, near coincident to an ERS 1 overpass (Figure 3b). Indicated are (top) temperature and (bottom) salinity. The section shows homogeneous Arctic Water in a 50- to 60-m deep layer below the grease ice. The shaded areas are the seafloor.

observing sea temperatures near the freezing point and lower salinities than in the surrounding water masses. Here bottom topography clearly played an important role in the circulation of the different water masses in this area, thus influencing where new ice will form. Whether this relationship holds for other parts of the Barents Sea is uncertain, especially given that the polar front is generally less well defined in the eastern Barents Sea [*Johannessen and Foster*, 1978; *Pfirman et al.*, 1994]. Also uncertain from our case study is how strongly bathymetry controls new ice formation under wind conditions different than those observed during the experiment. *Harris et al.* [1998] speculate that interannual variations in surface wind mixing affect the extent of sea ice in the Atlantic Water region such that the relationship between the sea ice formation and local water modification is affected; this clearly suggests a smaller degree of general bathymetric control.

The observed influence of grease ice on ERS 1 SAR backscatter suggests that satellite SAR may be useful for identifying new ice areas. The signatures identified using SIZEX92 data indicate image segmentation errors occur only in the presence of very low winds (< 2-3 m s^{-1}), which would result in open water backscatter comparable to that of grease ice; such low wind speeds were not observed during SIZEX92 and are not common in the Barents Sea in winter. Assuming the backscatter signatures are stable, SAR data may be applied to determine, for example, how far the grease ice zone may extend from the pack-ice edge, as well as identify regions that are significant zones of grease ice production. A limiting factor for systematically mapping the spatial and temporal variability of new ice areas may be the 3- or 6-day repeat cycles for satellites such as ERS. However, improvements in temporal sampling may be achieved by using wide-swath SAR such as the Radarsat ScanSAR or synergetic satellite SAR, as demonstrated during the 1996 ERS 1/ERS 2 SAR tandem operation with a 24-hour repeat time.

5. Ice Edge Definition and Variability

In addition to being important for practical purposes such as fisheries, offshore and transport operations, the position of the ice edge and its movement are important geophysical and biological variables. Geophysically, they are important parameters for investigations of sea ice dynamics and thermodynamics [e.g., *Johannessen et al.*, 1994], as well as climatological studies, since the ice edge serves to define ice extent in regional or hemispheric analyses [e.g., *Gloersen et al.*, 1992; *Johannessen et al.*, 1995]. Biologically, the ice edge regions are the most important in the polar oceans, especially in spring and summer, when phytoplankton superblooms and subsequent biological activity are greatest [*Smith and Niebauer*, 1993]. The ice edge definition and variability were studied using ERS 1 SAR data, in situ, and aerial observations obtained during SIZEX92.

5.1. Ice Edge Definition

A definition of the ice edge is necessarily subjective, as the marginal ice zone is a transition zone between open water and areas of dense pack ice. Physically, the ice edge can be either well defined or diffuse, straight or meandering, with ice eddies and ice tongues extending into open water areas, as has been demonstrated in previous field studies in the Barents and Greenland Seas [*Johannessen et al.*, 1987, 1992, 1994; *Sandven and Johannessen*, 1993]. The nominal ice edge is defined arbitrarily, most often as the 15% ice concentration isopleth in climatological studies. These studies usually use satellite passive microwave data with 25-km resolution. This relatively coarse resolution limits their precision (thus minimizing their usefulness for small-scale studies of ice edge variability) and can be an error source even for hemispheric-scale climatological analyses. A remote-sensing research goal is to use the higher-resolution satellite SAR data alone or in combination with passive microwave data, to better discriminate the ice edge.

During SIZEX92, the ice edge was observed to be sharp and nearly straight on March 2, 1992. The ERS 1 SAR image (Figure 3a) from that date also shows a distinct ice edge, defined here as the pack-ice edge, rather than the maximum extent of the grease ice. The backscatter profile (derived from three-pixel-wide transects on the 100 m resolution SAR image data) across the ice edge increased from about -13 dB in the first-year ice to about -4.5 dB in open water (Figure 9a). In this case, the application of an edge detection algorithm to the SAR data would accurately identify the ice edge without problem. However, in many cases, the ice edge is less distinct, with a rather diffuse transition from areas of higher to lower ice concentration.

The ice edge was meandering and relatively diffuse on March 8, 1992, owing to variable wind conditions. An 8 km wide swath of aerial photography was taken from the ice edge

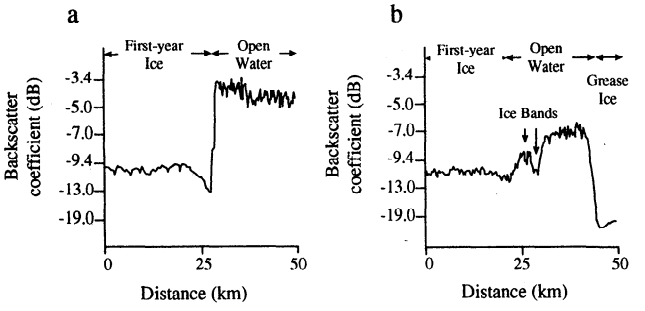

Figure 9. ERS 1 SAR backscatter profiles across the Barents Sea ice edge on March (a) 2 and (b) 8, 1992, during SIZEX92. For locations on the SAR images, refer to Figure 3.

northward 150 km into the interior of the ice pack. The capability of defining the ice edge by SAR was studied by comparing an excerpt of a three-look full-resolution image (16 x 20 m pixel) with aerial photography (Figure 10). The aerial photograph shows that the ice edge consists first of a 2-km-wide band of small (< 5 m in diameter) floes across the swath in the lower part of the photograph. Inside of (above) this band, a 4-5 km zone of mostly open water is found with some scattered bands of ice floes typically 100 m wide. North of the open water band, the ice pack consists of almost 100% concentration of small floes.

The full-resolution SAR image, which covers the same area as the aerial photo, shows two main features: open water in the lower part of the image gives higher backscatter than areas which are partly ice covered, and long surface waves from the south penetrate into the ice pack. The ice edge band is evident in the lower part of the image, but most of the smaller bands in the middle of the aerial photo are more difficult to observe in the SAR image. The darker spot near the center of the SAR image, corresponding to some open water within the ice edge band, could be explained by low wind and the absence of short surface waves in the smaller patches of open water between the ice floes. Without short surface waves there is no Bragg scattering that gives the high backscatter typically found in open water such as in the lower part of the SAR image. The SAR backscatter profile across the ice edge zone shows a less-pronounced gradient (3 dB) between the compact first-year ice and the open water (Figure 9b). Inside the ice edge, the profile shows the alternating bands of ice floes and open water that were observed in situ. Outside the ice edge, the profile shows a strong, 13 dB gradient between open water and grease ice, which had formed in the preceding days. In this case, an edge detection algorithm would find several edges, the most dominant of which is not the main ice edge between the first-year ice and open water. Investigations from the Kara Sea along the northern sea route [*Kloster et al.*, 1992a] and from SIZEX91 north of Svalbard [*Frette et al.*, 1992] found that this edge detection problem is exacerbated under summer conditions, with a relatively diffuse ice edge and the presence of wet ice, which reduces SAR backscatter.

5.2. Ice Edge Variability

Despite the above limitations, ERS 1 SAR data are complementary if not advantageous over other satellite data for detailed mapping of the ice edge. The variability and development of the ice edge region can be studied in detail using sequential ERS 1 SAR images. This was done during SIZEX92 when in situ and aerial observations were made for validation. Twenty SAR scenes were acquired from the same descending swath at 3-day intervals from March 2 to 11, 1992; refer to Figure 3 for the eight scenes covering the ice edge.

The ice edge on March 2, 1992, was remarkably well defined and nearly straight owing to southeasterly (on-ice) winds of 6-8 m s^{-1} during the preceding days. The SAR image shown in Figure 3a distinguishes clearly between open

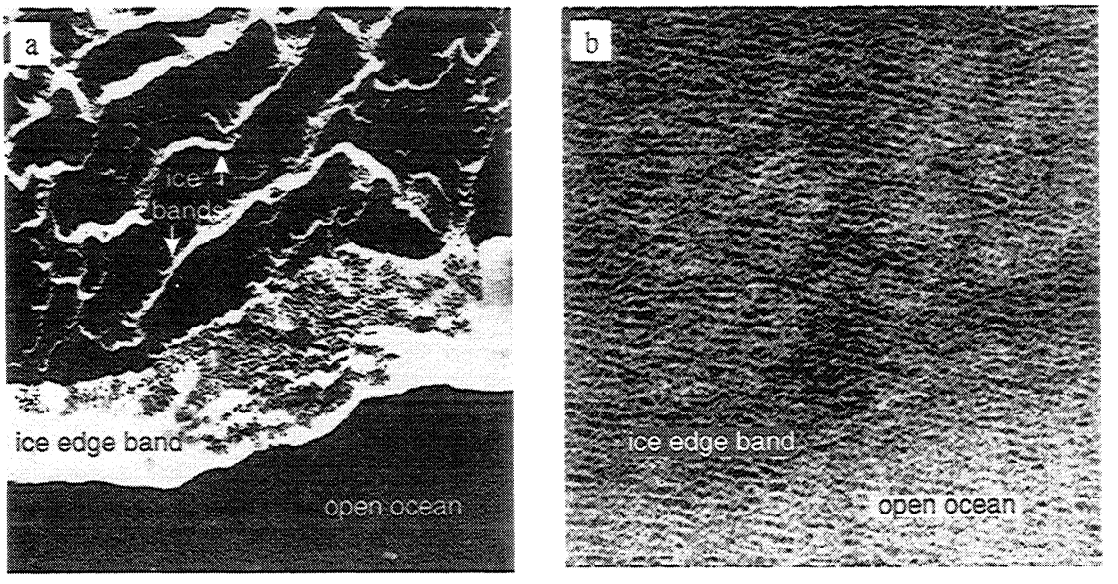

Figure 10. (a) Aerial photograph covering an 8- x 8-km area of the ice edge region taken on March 8, 1992, a few hours after an ERS 1 overpass. (b) Excerpt from a full-resolution ERS 1 SAR image (20-m pixel size) covering the same area as the aerial photograph. Indicated are alternating bands of ice floes and open water. ERS 1 SAR data are © ESA 1992.

water and compact ice (i.e., the ice edge) and the grease ice areas outside the ice edge. Owing to predominantly southwesterly winds between March 2 and 5, 1992, the ice edge became meandering and less well defined (Figure 3b). The area of newly forming ice outside the main ice edge expanded considerably in this period, and much of the grease ice had changed into pancake ice within 24-48 hours, based on our in situ observations. The distinction between grease ice (dark signature) and pancake ice (bright signature) is clear on the March 5, 1992, SAR image (Figure 3b). The continued reconfiguration and relocation of the ice edge is evident in the SAR images from March 8 and 11, 1992 (Figures 3c and 3d). Moderate (4-6 m s^{-1}) off-ice winds caused bands of small floes parallel to the main ice edge, but these bands were not clearly evident on the SAR images.

The SIZEX92 in situ observations and ERS 1 SAR data confirm earlier observations [*Johannessen et al.*, 1992] that the winter ice edge in the Barents Sea is extremely complex and variable, as a result of both dynamic and thermodynamic forcings. The ERS 1 SAR data were proven excellent for studying the small-scale spatial variability and patterns, but the temporal resolution provided by the 3-day repeat cycle for ERS-1 is insufficient to study the even more rapid development of the ice edge, such as that seen previously using airborne SAR [*Johannessen et al.*, 1991]. Thus the spatiotemporal sampling limitations of satellite SARs such as ERS for ice edge studies are similar to those for mapping new ice areas (section 4).

6. Ice Types and Ice Floes

The objective of the *Polarsyssel* cruise was to make observations of ice types and ice floe characteristics (size, thickness, and surface character) within the ice edge, nearly coincident with ERS 1 overpasses. This part of SIZEX92 was especially dedicated to ERS 1 SAR validation, i.e., to provide an in situ data set for backscatter signature studies. The technical details can be found in the remote-sensing literature, e.g., *Sandven and Johannessen* [1993] and SIZEX92 technical reports, e.g., *Sandven et al.* [1993]. Here we briefly summarize the observations of geophysical interest, with reference to ERS 1 SAR.

6.1. Ice Type Classification from SAR Data

During SIZEX92, a range of new (including grease ice, pancake ice, and young ice), first-year and multiyear ice types were present in the study area. A detailed set of *in situ* snow and ice measurements were made, nearly coincident with ERS 1 overpasses. Forty-one ice cores were obtained from 21 sites on large first-year and multiyear ice floes. At each site, measurements of ice thickness, temperature, salinity, density, brine volume, and structure were made, and the surface roughness was characterized qualitatively. Ice type was identified based on these data. These observations were useful per se and were the basis for developing a set of ERS 1 SAR backscatter signatures for the Barents Sea in winter. The SIZEX92 backscatter statistics were derived using image analysis software to define polygons and calculate the mean and standard deviation for σ_0 in the area defined. The polygons ranged from about 2-8 km across and each contained between about 400 and 4000 pixels. Representative backscatter ranges were derived from the statistics from several polygons defined for each ice type, as well as open water under various conditions.

The ice edge zone had a combination of open water and various stages of new and first-year ice types. The open water areas usually had a higher backscatter than any of the ice types, ranging from -4.5 to -3.0 dB. The initial freezing stage results in grease ice (section 4.1 and Figure 5), which had the lowest backscatter of all ice types, from -24 to -14 dB. The grease ice was seen to develop rapidly into pancake ice with sharp edges and high (> -7.0 dB) backscatter. Also observed were small floes of thicker first-year ice, continually exposed to surface waves and therefore rough, with a backscatter between -10.5 and -6.5 dB.

The intermediate zone during SIZEX92 was 20-30 km wide, with high (> 95%) ice concentration. It was characterized by small floes, typically 10-100 m across; the floes appeared to have been broken up by surface waves penetrating from the open ocean. The dominant ice type was deformed first-year ice about 2 m thick owing to the "rafting" of floes, with a rough surface and backscatter values between -10 and -6.5 dB.

The interior zone was characterized by large areas of first-year and multiyear ice, especially north of 78°N. Between the large multiyear floes were areas of consolidated first-year ice, typically 2-3 m thick. These ice types had typical backscatter values of -9.0 ±1.5 and -10 to -13 dB, respectively. In situ measurements were made at four sites on a very large (10 km) multiyear ice floe, and an interpretation of its SAR image backscatter indicates that each of the larger multiyear floes was essentially a deformed coalescence of smaller floes.

Besides any geophysical significance, the existence of these zones has negative implications for general ice classification based on SAR data. Moreover, it should not be presumed that ERS 1 SAR signatures in the Barents Sea in winter are valid elsewhere; indeed, there is only partial agreement between the signatures derived in SIZEX92 and other earlier analyses, as summarized by *Onstott* [1992]. Both regional and seasonal reference tables must be developed before ERS 1 SAR ice classification can be made reliable. Toward this end, the results of the SAR backscatter studies of the different ice types observed primarily in SIZEX92 and secondarily from earlier experiments are summarized in Figure 11. The separation of ice types based on backscatter intervals was done for different areas and seasons. The seasonal differences may be large; e.g., melt effects in summer can lower the backscatter values observed in winter. For the winter conditions in SIZEX92, we have distinguished the interior zone from the intermediate ice edge region because it may be useful to separate different types of ice that have similar backscatter intervals. For example, multiyear ice in the interior can have similar backscatter as small and medium floes of first-year ice in the ice edge region, whereas pancake ice in the ice edge region can have similar backscatter as ridged and heavily deformed first-year and multiyear ice in the interior. Thus ice classification based solely on ERS SAR backscatter in the seasonal ice zone or MIZ is more challenging than the perennial pack ice.

An automated ice classification algorithm developed for the MIZ has been applied to the SIZEX92 data, an example of which is shown in Plate 1. The image segmentation, where each region is assigned to a different ice type, was done using the *Wackerman and Miller* [1996] algorithm. Their goal is to eventually be able to reliably apply such an algorithm to any

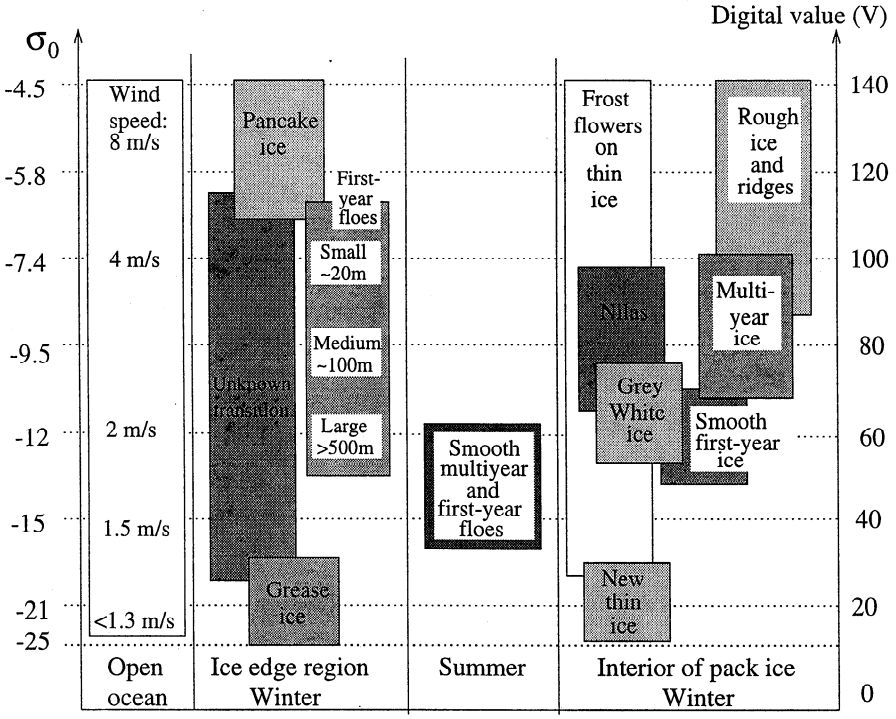

Figure 11. Schematic diagram summarizing SAR backscatter for different ice types studied in SIZEX92 and previous experiments. The σ_0 values are based on the empirical relationship: $\sigma_0 = 20 \log V - 46.9$, assuming that $V = 14$ corresponds to a noise floor of -24 dB. V is the digital value of the image data received from the Tromsø Satellite Station.

ERS SAR image acquired in the MIZ. The algorithm uses both statistics and texture (namely, measures of decorrelation and co-occurrence) to find the optimal separation between pixel classes. *Wackerman and Miller* [1996] found about 80% accuracy in their cases from the Barents Sea MIZ, mostly due to the statistics rather than the texture measures.

Here three scenes from the March 5 SAR swath were selected because they included each of the different ice types that were investigated in the field. Before the classification could be done, the knowledge of the characteristic ice types based on in situ observations was used to select a few training areas for each class. In this example, six classes were selected: open water, grease ice, pancake ice, deformed first-year ice (including congealed pancake ice), nondeformed first-year ice, and multiyear ice.

The overall results (Plate 1) appear reasonable, but some incorrect classifications are evident. An obvious error is the pancake ice classification amid multiyear ice in the interior of the ice pack, probably due to scattering from ridges. Conversely, there were also incorrect multiyear classifications in the pancake ice area. The nondeformed first-year ice classified in the new ice area is also incorrect, as documented by in situ observations in the area. Another questionable result is the occurrence of open water inside the new ice area, where it is probably pancake ice or rafted nilas/young ice, though there were no in situ observations to confirm this. In spite of these errors, it is promising that the deformed first-year ice, grease ice, and open water, as well as pancake ice in the MIZ, are very well classified, considering that this example is difficult to classify. In developing the classification technique further, the probability of ice types that can occur in each zone could be included; introduction of such knowledge should remove some of the errors evident in Plate 1. Nonetheless, automated MIZ ice classification using single-channel SAR may prove intractable, even when texture measures are incorporated into the classification algorithm.

6.2. Ice Floe Identification from SAR Data

Ice floe characteristics are of geophysical and applied interest, though few studies address the characterization problem [e.g., *Weeks et al.*, 1980; *Rothrock and Thorndike*, 1984]. The ability to retrieve floe parameters such as size and shape from satellite SAR data would be an advancement. An investigation into floe identification and floe size distribution was made during SIZEX92, using in situ and low-altitude airplane and helicopter observations, and high- (25 m) and low-resolution (100 m) ERS 1 SAR data. The *Polarsyssel* was located 30 km north of the ice edge at 77°5'N, 30°E on March 8, 1992. From there, a helicopter made two excursions from the ice edge to 78°N and one in the ice edge region. From the helicopter, visual reconnaissance and downward looking video records were made, coincident with a series of low-altitude aerial photographs and ERS 1 SAR images.

A qualitative analysis of the aerial photographs and helicopter records revealed the floe size distribution near the ice edge to be bimodal. Proceeding from the ice edge into the interior of the ice pack, the distribution remained bimodal to about 50 km from the ice edge. The mean floe diameter (based on the long and short axes) increased exponentially from less than 10 m near the ice edge, to about 40 m 25 km from the ice edge (Figure 12a), to about 120 m 50 km from the ice edge.

The possibility of identifying ice floes from SAR images was studied by comparing the SIZEX92 aerial photographs

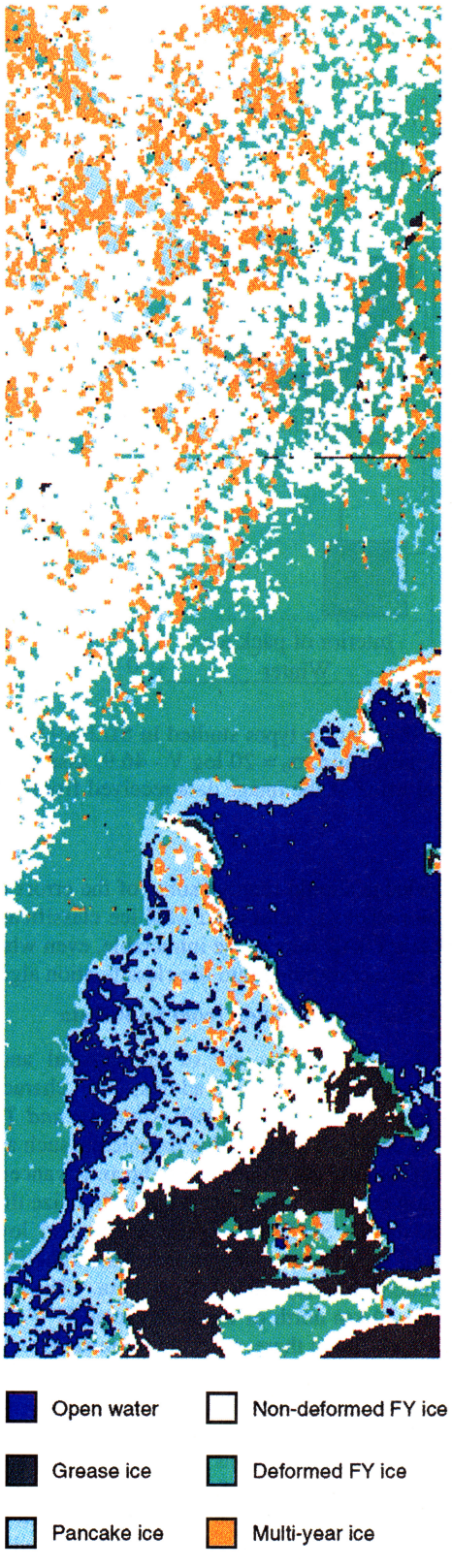

Plate 1. Color-coded sea ice classification of ERS 1 SAR image data (100 x 300 km) from March 5, 1992, based on the *Wackerman and Miller* [1996] algorithm, which uses both statistics and textures measures to separate the pixel classes. Original ERS 1 SAR data are © ESA 1992.

with full-resolution ERS 1 SAR images. The SAR data were incapable of resolving the floes near the ice edge, where the floe size was of order 10 m or less (Figure 10). The situation is identical at about 20 km into the ice pack (Figure 12a), where the floe size was about 20 m, similar to the pixel size of the full-resolution SAR image (Figure 12b). The SAR data were, however, able to detect a 100-m tabular iceberg by its bright return (Figure 12b).

At about 60 km north of the ice edge, where the ice regime changes from small floes broken up by waves to larger floes unaffected by waves, the floe sizes were up to 1-3 km with some open water/new ice between the floes (Figure 13a). Despite the large floe size, they are difficult to resolve unambiguously in the SAR images (Figure 13b). This is particularly true when ice concentration is above 90% and the floes are densely clustered so that the SAR cannot detect space between the floes (e.g., F_1-F_4 in Figure 13). The floes can best be detected when there are leads that are hundreds of meters across, such as those indicated L_1 and L_2 in Figure 13a. This is illustrated by the SAR image in Figure 13b.

In the interior of the ice pack, where larger floes predominate, SAR data may be useful in studying the geometry and distribution of floe sizes if the boundaries are well delineated, as well as ice motion based on floe recognition (section 7). In this case, at distances greater than 60 km from the ice edge, there was a rapid increase in floe size to above 1 km, which the SAR could detect only where the floes were surrounded with sufficiently large leads. In this region were found numerous large multiyear floes up to 3-4 km across, which were qualitatively identifiable on the SAR images, based on their size and high backscatter.

7. Ice Motion in the Marginal Ice Zone

The variability of the ice edge in response to atmospheric forcing was seen earlier in the March 2-11 ERS 1 SAR image sequence (Figure 3). The ability to use sequential SAR images to derive ice motion fields was investigated using the SIZEX92 SAR data and in situ measurements. The darkness and cloud independence of SAR, as well as its higher resolution, suggest that satellite SAR data should be useful for systematic derivation of ice motion fields. Several ice motion algorithms, based on feature recognition and correlations between paired image features, have already been developed and tested on various satellite data sets [e.g., *Fily and Rothrock*, 1990; *Kwok et al.*, 1992]. For SIZEX92, we adapted and applied an ice motion algorithm developed by *Kloster et al.* [1992b] to sequential ERS 1 SAR data from the western Barents Sea. On the basis of the same principles as other ice motion algorithms, the algorithm applies a two-dimensional binary search in pairs of subimages to reduce the total number of correlations to be estimated.

It was applied to same-swath, sequential SAR images at 3- and 6-day intervals in the 5-week period preceding SIZEX92 (not shown) and at 3-day intervals during the experiment. A notable result of the SAR ice motion studies was the inability to obtain any reliable results in the intermediate ice edge zone (zone B in Figure 4) and in areas of new ice formation (zone C in Figure 4). The reason is that it is difficult to find any features that can be correlated in these areas of the SAR images, an obvious requirement for calculating ice motion.

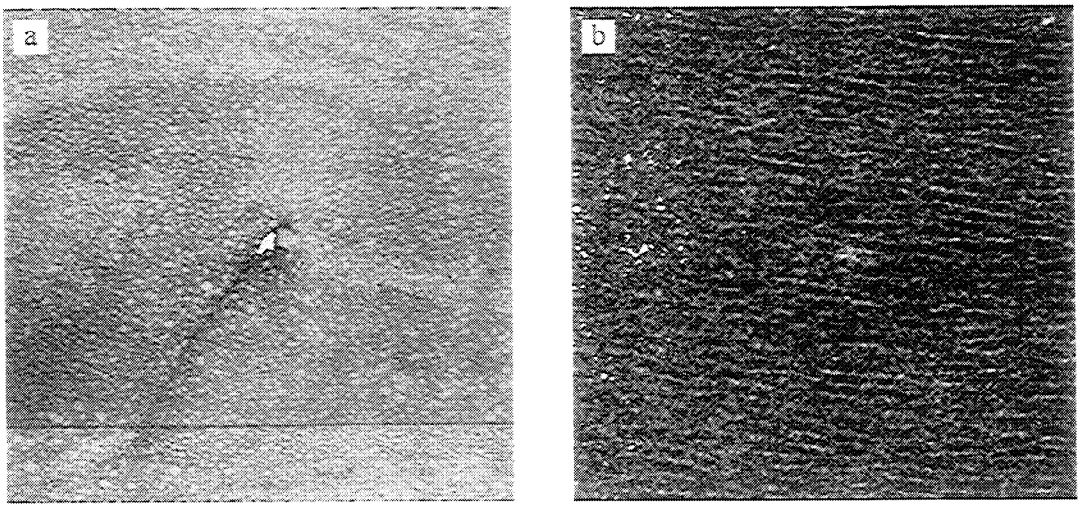

Figure 12. (a) Aerial photograph of a 2- x 2-km area taken on March 8, 1992, about 20 km into the ice edge, indicated by the middle square in Figure 3c. The photograph shows a drifting iceberg about 100 m in diameter moving toward the southwest at a slower speed than the surrounding pack ice, as indicated by the wake. Typical floe sizes of the pack ice are 10-20 m. (b) Excerpt from a same-date full-resolution ERS 1 SAR image covering the same area as the photograph. ERS 1 SAR data are © ESA 1992.

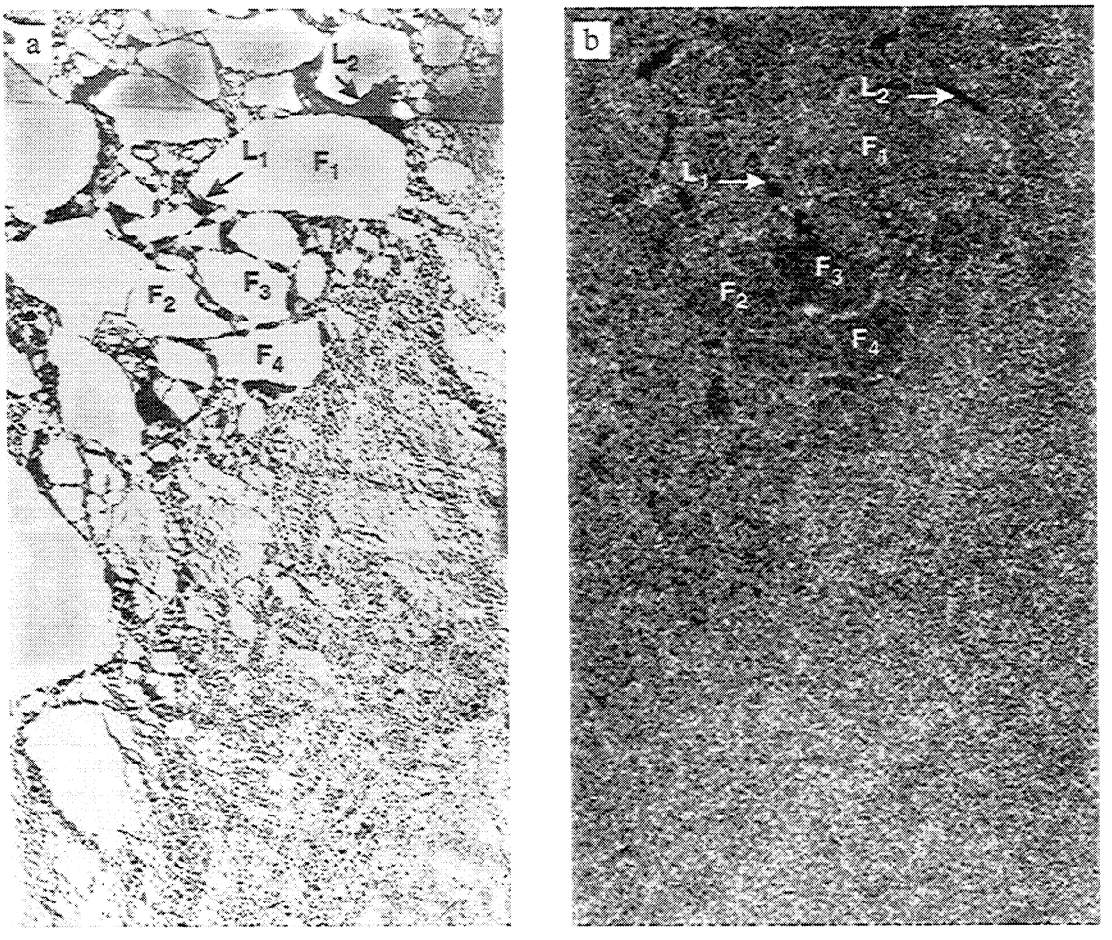

Figure 13. (a) Aerial photograph of an 8- x 15-km area in the transition area between the interior of the ice pack and an intermediate zone taken on March 8, 1992, indicated by the top square in Figure 3c. (b) Excerpt from a same-date full-resolution SAR scene covering the same area as the photograph at the same scale. Identical floes (F_1) and leads (L_1) common to each image are identified. The ERS 1 SAR data are © ESA 1992.

In the interior (zone A in Figure 4), the SAR-derived ice velocity vectors were numerous and appeared reasonable, though no validation data were available during this period.

During the experiment period, the ice velocity vectors derived from SAR could be compared with independent in situ measurements from Argos buoys deployed between the ice edge region and the interior of the ice pack at about 79°N. The Argos system provided buoy positions every 3 hours. These positions were low-pass filtered to remove tidal motion from the ice drift. The positioning uncertainty is only ±500 m d^{-1}, such that the 3-day errors are considered negligible.

For the interior of the ice pack, the algorithm appears to give reasonable, coherent results for the 3-day period March 8-11 (thin arrows in Figure 14), which also shows the nearly complete absence of vectors in the intermediate zone (Figure 14, bottom right). However, there are error sources that can have a significant impact on the SAR-derived ice motion estimates, the most important being image geolocation. Compared to the drifting buoy vector (thick arrow in Figure 14) the SAR-derived vectors (thin arrows) are too short and are rotated clockwise about 20°. This discrepancy is believed to be caused by an error in the geolocation of the March 11 image. Because none of the SAR images used in the calculations could be geolocated using fixed land points, our only means to check the image positions given by the Tromsø Satellite Station (TSS) was to find positions of known image features using ships or helicopters. For the March 11 image, no such positions were available. The effect of geolocation errors can be illustrated as follows: if the March 11 image is relocated some 5-10 km along the orbit toward the south, the y coordinates of the ice velocity vectors would be increased by the same distance and the vectors would be in agreement with the Argos-derived vector. The geocoding metadata provided by TSS with the near-real-time SAR data used in SIZEX92 are not as accurate as those provided by ESA with its "on-line" products, such that precaution must be taken when using SAR data in near real time.

8. Conclusions

The SIZEX92 experiment provided ERS 1 SAR validation data as well as insight into the nature of the Barents Sea seasonal ice zone in winter. In particular, insight was gained into ice edge features and processes, including the formation of new ice and its relationship to water masses and bottom topography. The new ice areas were seen to correspond with the shelf break through its influence on the local circulation of Arctic and Atlantic Water. The ERS 1 SAR demonstrated its capability to map areas of new ice formation based on the dampening effect of grease ice on radar backscatter. The ERS 1 SAR's high resolution provided detailed information on the position and configuration the ice edge; image sequences revealed rapid, mesoscale variations in new ice areas and the ice edge in response to wind conditions.

SIZEX92 also provided information and validation data to assess ERS 1 SAR's capabilities for retrieving sea ice parameters within the ice pack. Proceeding from the ice edge to the interior, a changing amalgam of ice floe characteristics and ice types was observed in situ and from aerial photographs. In each case, ERS 1 SAR was seen to provide at least qualitative information on ice characteristics. However, the SIZEX92 experience suggests that although some improvements are expected with further research, automated parameter retrieval such as ice floe identification and ice classification in the MIZ remains problematic. Sequential ERS 1 SAR data were seen to be useful for ice motion in the interior of the ice pack, less so for the area intermediate to the ice edge zone. Moreover, the accuracy of ice motion fields derived from sequential SAR data, in the absence of fixed reference locations and/or independent validation data,

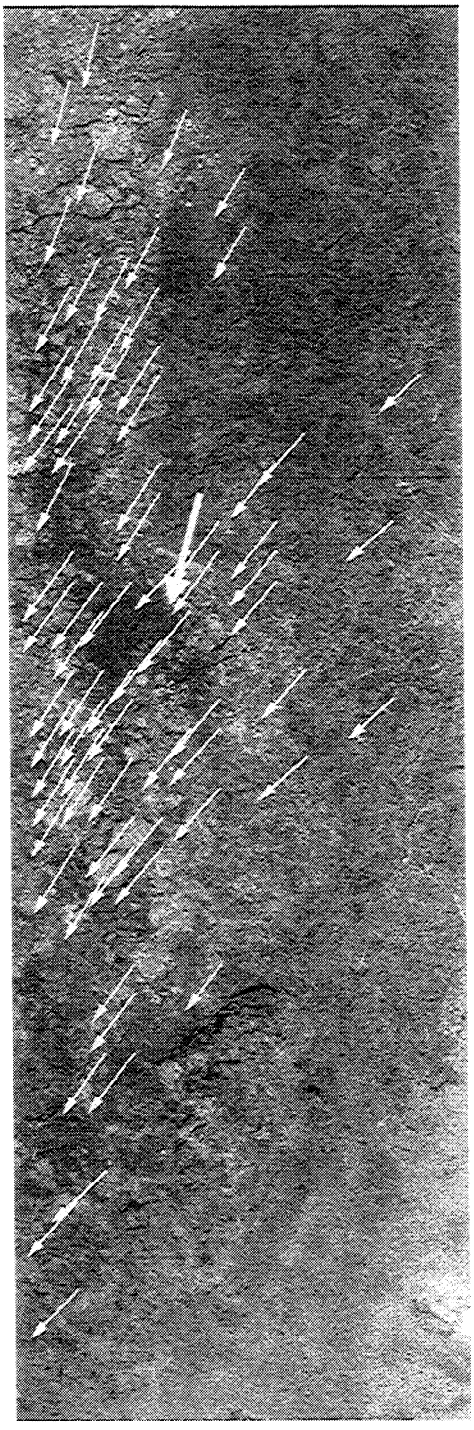

Figure 14. Ice motion vectors derived from a pair of ERS 1 SAR image strips (March 8 and 11, 1992), indicated by thin arrows, and an independent drift vector (thick arrow) obtained from Argos buoy position data. The differences in the vectors and the absence of arrows at bottom right are explained in the text. The ERS 1 SAR data are © ESA 1992.

depends on accurate navigation metadata, which should not be assumed.

Acknowledgments. This research was done under contract from the European Space Agency ESA-ESTEC (contract 9969/92/NL/US), the Norwegian Space Centre (contract JOP.8.33.0692.2), and the Norwegian Research Council's Strategic Program on "SAR imaging of ocean and ice phenomena" (contract 107628/420). The SIZEX92 experiment itself was also supported by the Operatørkomite Nord (OKN), the Office of Naval Research (ONR), and the University of Bergen, Norway. The authors thank personnel from the Environmental Research Institute of Michigan (ERIM), the Naval Postgraduate School in Monterey, the United States Geological Survey (USGS) in Tacoma, and FORUT in Tromsø, Norway, for their contributions to the experiment. The authors also thank Torill Hamre, Øyvind Dalen, Lars Viljar Kvavik, and Maria Lundhaug at NERSC for data processing assistance.

References

Aagaard, K., and E. C. Carmack, The role of sea ice and other fresh water in the arctic circulation, *J. Geophys. Res., 94*, 14,485-14,498, 1989.

Alekseev, G. V., V. V. Ivanov, and A. A. Korablev, Interannual variability of the thermohaline structure in the convective gyre of the Greenland Sea, in *The Polar Oceans and Their Role in Shaping the Global Environment, Geophys. Monogr. Ser.*, vol. 85, edited by O. M. Johannessen et al., pp. 485-496, AGU, Washington, D. C., 1994.

Carlström, A., and L. M. H. Ulander, Validation of backscatter models for level and deformed sea-ice in ERS-1 SAR images, *Int. J. Remote Sens., 17*, 3287-3306, 1995.

Fily, M., and A. Rothrock, Opening and closing of sea ice leads: Digital measurements from synthetic aperture radar, *J. Geophys. Res., 95*, 789-796, 1990.

Frette, Ø., S. Sandven, O. M. Johannessen, K. Korsnes, and B. Erlingsson, In situ observations of sea ice during the Lance cruise in August 1991, *Spec. Rep. 13*, Nansen Environ. and Remote Sens. Cent., Bergen, Norway, 1992.

Gloersen, P., W. J. Campbell, D. J. Cavalieri, J. C. Comiso, C. L. Parkinson, and H. J. Zwally, Arctic and Antarctic sea ice, 1978: Satellite passive-microwave observations and analysis, *NASA Spec. Publ. SP-511*, 1992.

Gloersen, P., J. Yu, and E. Mollo-Christensen, Oscillatory behavior in Arctic sea ice concentrations, *J. Geophys. Res., 101*, 6641-6650, 1996.

Gudmandsen, P., B. B. Thomsen, L. T. Pedersen, H. Skriver, and P. J. Minnett, North-East Water polynya: satellite observations summer 1992 and 1993, *Int. J. Remote Sens., 17*, 3307-3324, 1995.

Harris, C. L., A. J. Plueddemann, and G. G. Gawarkiewicz, Water mass distribution and polar front structure in the western Barents Sea, *J. Geophys. Res., 103*, 2905-2917, 1998.

Johannessen, J. A., O. M. Johannessen, S. Sandven, and P. M. Haugan, A characterization of air-sea-ice interactive processes in the MIZ, based on SAR-derived ice edge configurations, in *Proc. IGARSS '91*, pp. 429-432, Eur. Space Agency, Helsinki, 1991.

Johannessen, O. M., and L. A. Foster, A note on the topographically controlled oceanic front in the Barents Sea, *J. Geophys. Res., 83*, 4567-4571, 1978.

Johannessen, O. M., W. J. Campbell, R. Shuchman, S. Sandven, P. Gloersen, J. A. Johannessen, E. G. Josberger, and P. M. Haugan, Microwave study programs of air-sea-ice interactive processes in the seasonal ice zone of the Greenland and Barents seas, in *Microwave Remote Sensing of Sea Ice, Geophys. Monogr. Ser.*, vol. 68, edited by F. Carsey, pp. 261-289, AGU, Washington, D. C., 1992.

Johannessen, O. M., J. A. Johannessen, E. Svendsen, R. A. Shuchman, W. J. Campbell, and E. G. Josberger, Ice edge eddies in the Fram Strait marginal ice zone, *Science, 236*, 427-429, 1987.

Johannessen, O. M., S. Sandven, W. P. Budgell, J. A. Johannessen, and R. A. Shuchman, Observation and simulation of ice tongues and vortex pairs in the marginal ice zone, in *The Polar Oceans and Their Role in Shaping the Global Environment, Geophys. Monogr. Ser. 85*, edited by O.M. Johannessen et al., pp. 109-136, AGU, Washington, D. C., 1994.

Johannessen, O. M., M. W. Miles, and E. Bjørgo, The Arctic's shrinking sea ice, *Nature, 376*, 126-127, 1995.

Kloster, K., O. M. Johannessen, S. Sandven, and Ø. Frette, The Northern Sea Route: analysis of ERS-1 SAR data from August 1991, *Spec. Rep. 2*, Nansen Environ. and Remote Sens. Cent., Bergen, Norway, 1992a.

Kloster, K., H. Flesche, and O. M. Johannessen, Ice motion from airborne SAR and satellite imagery, *Adv. Space Res., 12*(7), 149-153, 1992b.

Kwok, R., E. Rignot, and B. Holt, Identification of sea ice types in spaceborne synthetic aperture radar data, *J. Geophys. Res., 97*, 2391-2402, 1992.

Laur, H., P. Bally, P. Meadows, J. Sanchez, B. Schaettler, and E. Lopinto, ERS SAR calibration: Derivation of the backscattering coefficient s_0 in ESA ERS PRI products, *Publ. ES-TN-RS-PM-HL09, 2*(4), Eur. Space Res. Inst., Frascati, Italy, 1997.

Loeng, H., Features of the physical oceanographic conditions of the Barents Sea, *Polar Res., 10*, 5-18, 1991.

Midttun, L., Formation of dense bottom water in the Barents Sea, *Deep Sea Res., Part A, 32*, 1233-1241, 1985.

Midttun, L., Climatic fluctuations in the Barents Sea, *Rapp. P.V. Reun. Cons. Int. Explor. Mer. Mediter., 188*, 23-35, 1989.

NORSEX Group, Norwegian remote sensing experiment in the marginal ice zone, *Science, 220*, 781-787, 1983.

Onstott, R. G., SAR and scatterometer signatures of sea ice, in *Microwave Remote Sensing of Sea Ice, Geophys. Monogr. Ser.*, vol. 68, edited by F. Carsey, pp. 73-104, AGU, Washington, D. C., 1992.

Parkinson, C. L., Interannual variability of the spatial distribution of sea ice in the north polar region, *J. Geophys. Res., 96*, 4791-4801, 1991.

Pfirman, S. L., D. Bauch, and T. Gammelsrød, The northern Barents Sea: water mass distribution and identification, in *The Polar Oceans and Their Role in Shaping the Global Environment, Geophys. Monogr. Ser.*, vol. 85, edited by O. M. Johannessen et al., pp. 77-94, AGU, Washington, D. C., 1994.

Rogers, J. C., and E. Mosley-Thompson, Atlantic arctic cyclones and the mild Siberian winters of the 1980s, *Geophys. Res. Lett., 22*, 799-802, 1995.

Rothrock, D. A., and A. S. Thorndike, Measuring the sea ice floe size distribution, *J. Geophys. Res., 89*, 6477-6486, 1984.

Sandven, S., and O. M. Johannessen, Ice studies in the Barents Sea by ERS-1 during SIZEX92, *Adv. Space Res., 13* (5), 41-52, 1993.

Sandven, S., K. Kloster, O. M. Johannessen, and M. Miles, SIZEX92: ERS-1 SAR ice validation experiment, *Tech. Rep. 69*, Nansen Environ. and Remote Sens. Cent., Bergen, Norway, 1993.

Smith, W. O., Jr., and H. J. Niebauer, Interactions between biological and physical processes in Arctic seas: Investigations using numerical models, *Rev. Geophys., 31*, 189-209, 1993.

Vinje, T., Drift, composition, morphology and distribution of the sea ice fields in the Barents Sea, *Publ.. 179C*, 26 pp., Norw. Polar Res. Inst., Oslo, 1985.

Vinje, T., and Å. S. Kvambekk, Barents Sea drift ice characteristics, *Polar Res., 10*, 59-68, 1990.

Wackerman, C., and D. Miller, An automated algorithm for sea ice classification in the marginal ice zone using ERS-1 Synthetic Aperture Radar, *Rep. 252000-25-T*, 49 pp., Environ. Res. Inst. of Mich., Ann Arbor, 1996.

Weeks, W. F., W. B. Tucker, M. Franck, and S. Fungcharoem, Characterization of surface roughness and floe geometry of sea ice over the continental shelves of the Beaufort Sea and Chukchi Seas, in *Sea Ice Processes and Models*, edited by R. S. Pritchard, pp. 300-312, Univ. of Wash. Press, Seattle, 1980.

O. M. Johannessen, K. Kloster, M. W. Miles, L. H. Pettersson, and S. Sandven, Nansen Environmental and Remote Sensing Center, Edvard Griegsvei 3a, 5059 Bergen, Norway. (stein.sandven@nrsc.no)

(Received October 26, 1997; revised August 3, 1998; accepted September 9, 1998.)